LaMn$_{1-x}$Fe$_x$O$_3$ and LaMn$_{0.1-x}$Fe$_{0.90}$Mo$_x$O$_3$ Perovskites: Synthesis, Characterization and Catalytic Activity in H$_2$O$_2$ Reactions

Fabiano Magalhães[a], *Flavia Cristina Camilo Moura*[b], *José Domingos Ardisson*[c], *Rochel Montero Lago*[a]*

[a]*Departamento de Química, Universidade Federal de Minas Gerais,*
31270-901 Belo Horizonte - MG, Brazil
[b]*Departamento de Química, ICEB, Universidade Federal de Ouro Preto,*
35400-000 Ouro Preto - MG, Brazil
[c]*Laboratório de Física Aplicada,*
Centro de Desenvolvimento de Tecnologia Nuclear, CDTN-CNEN,
Av. Antônio Carlos, 6627, Belo Horizonte - MG, Brazil

In this work two perovskites were prepared: LaMn$_{1-x}$Fe$_x$O$_3$, and LaMn$_{0.1-x}$Fe$_{0.90}$Mo$_x$O$_3$. XRD and Mössbauer spectroscopy suggest the formation of pure phase perovskite with the incorporation of Fe and Mo in the structure. The catalytic activity of these materials was studied in two reactions with O$_2$: the decomposition to O$_2$, and the oxidation of the model organic contaminant methylene blue. The perovskite composition strongly affects the catalytic activity, while Fe decreases the H$_2$O$_2$ decomposition Mo strongly improves dye oxidation.

1. Introduction

The reaction of organic compounds with Fenton reagent is one of the most efficient methods for the destruction of organic contaminants in wastewaters. The classical Fenton system, a mixture of H$_2$O$_2$ and a Fe(II) salt, generates in situ free hydroxyl radicals according to the Haber-Weiss mechanism (Equation 1).

$$Fe^{2+} + H_2O_2 \rightarrow Fe^{3+} + {}^{\bullet}OH + OH^- \qquad (1)$$

The strong oxidizing hydroxyl radicals react with organic compounds in water leading to their mineralization to CO$_2$ and H$_2$O as the final harmless products.

Increasingly efficient heterogeneous Fenton-like systems have been investigated where soluble Fe^{2+} species is replaced by different iron oxides such as goethite, hematite and ferrihydrite.

Perovskites type oxides, ABO$_3$, have been extensively investigated as catalysts for several processes including fuel cells[1], water dissociation[2], hydrogenation, hydrogenolysis[3], ammonia oxidation[4] and NO$_x$ reduction[5]. Several reviews covering these fields can be found in the literature[6,7]. Perovskites, especially LaMnO$_3$, have also been used in environmental applications, e.g. the oxidation of hydrocarbons[8-10], chlorinated organics[11] and H$_2$O$_2$ reactions[6,12]. LaMnO$_3$ shows good stability, flexible oxygen stoichiometry (δ) and the different Mn oxidation states i.e. Mn^{2+}, Mn^{3+}, Mn^{4+}, which strongly affects the catalytic behavior. Also, isomorphic substitution of metals in the perovskite structure allows some control the catalytic properties of the material. Several LaMnO$_3$ derivatives, i.e. La$_{1-x}$A$_x$Mn$_{1-y}$M$_y$O$_3$ (where A is a lanthanide, actinide, alkaline or earth alkaline metal and M is another transition metal such as Co, Ni, etc.) have been previously investigated[13,14].

In this work, we studied the isomorphic substitution of Mn in the LaMnO$_3$ structure by different amounts of Fe and Mo to produce LaMn$_{1-x}$Fe$_x$O$_3$ and LaMn$_{0.1-x}$Fe$_{0.90}$Mo$_x$O$_3$. The Fe and Mo can also vary their oxidation states and this property can improve the catalytic activity in oxidation processes. These perovskites were characterized and the catalytic activity was investigated using two H$_2$O$_2$ reactions, i.e. the decomposition to O$_2$ and the oxidation of the dye methylene blue used as model contaminant.

2. Experimental

The perovskites were prepared by the reaction of 0.5 mol of citric acid (CA) dissolved in 2 mol of water at 60 °C, followed by the addition of 1 mmol of La(NO$_3$)$_3$.6H$_2$O and different proportions of the other metals such as x mmol Fe(NO$_3$)$_3$.9H$_2$O, y mmol Mn(NO$_3$)$_2$.4H$_2$O and z mmol Mo(acac)$_2$O$_2$ in order to produce the desired stoichiometry LaMn$_y$Fe$_x$Mo$_z$O$_3$. The mixture was stirred for about 2 hours, until a clear orange solution of the stable metal–CA complexes was obtained. After complete dissolution, 400 mmol of ethyleneglycol (EG) was added and the solution was continuously stirred while the temperature was slowly increased to 90 °C. This step removes the excess of water and allows the polyesterification reaction between CA and EG to be further activated. The heating at 90 °C over 7 hours resulted in a viscous orange resin.[12] This resin was then treated at 400-450 °C in air over 2 hours for the carbonization. The final product, a dark brown powder, was ground and then calcined at 800 °C in air for 6 hours.

The catalysts were characterized by XRD, TPR (temperature programmed reduction), Mössbauer spectroscopy, BET surface area and thermal analysis. The surface area was determined by the BET method using a 22 cycles of N$_2$ adsorption/desorption in an Autosorb 1 Quantachrome instrument. The Mössbauer spectroscopy experiments were carried out in the transmission geometry on a constant-acceleration conventional spectrometer with a ^{57}Co/Rh source at room temperature (RT) using α-Fe as a reference. The powder XRD data were obtained in a Philips X'Pert equipment using Cu Kα or Co Kα radiation scanning from 2 to 80° at a scan rate of 4° per minute. The TPR (temperature programmed reduction) analysis was performed

*e-mail: rochel@ufmg.br

in a CHEM BET 3000 TPR using H_2 (8% in N_2) with heating rate of 10 °C per minute. The H_2 consumption was obtained after calibration of the TPR system using a CuO standard. The thermal analysis was carried out in a SHIMADZU DTG-60, with a constant heating rate of 10 °C per minute under air flow (50 mL/min). The hydrogen peroxide (Synth) decomposition was carried out with 7 mL H_2O_2 (2.9 mol.L^{-1}) and 60 mg of catalyst. The formation of gaseous O_2 was measured in a volumetric glass system. All the reactions were carried out using magnetic stirring in a recirculating temperature controlled bath kept at 25 ± 1 °C. The oxidation of the methylene blue at the concentration of 0.05 g.L^{-1} with H_2O_2 was monitored by UV/Vis at 663 nm. During the reaction the pH varied from 5.5 up to 6.0 which does not change significantly the absorptivity of the dye. All the reactions were carried out using 30 mg of the catalyst in a recirculating temperature controlled bath at 25 ± 1 °C.

3. Results and Discussion

3.1. Characterization of the perovskites

The study of the crystalline phases present in the perovskites $LaMn_{1-x}Fe_xO_3$ and $LaMn_{0.1-x}Fe_{0.90}Mo_xO_3$ was carried out by XRD analyses (Figures 1 and 2).

The main peaks in Figure 1a are related to the perovskite phase, e.g. $LaMnO_3$ 2θ at 22.9, 32.6, 40.2, 46.9, 52.7, 58.1 and 68.2° [15], with crystal structures adjusted to a pseudo-cubic arrangement [16,17]. It can be observed, however, a gradual shift of the XRD peaks to lower diffraction angles as the Fe content increased with cell parameters increasing from 3.885(2) to 3.944(1) Å (a = b = c).

XRD results for the $LaFe_{0.90}Mn_{0.1-x}Mo_xO_3$ series (Figure 2) were very similar, showing a perovskite phase with the peak shift to lower
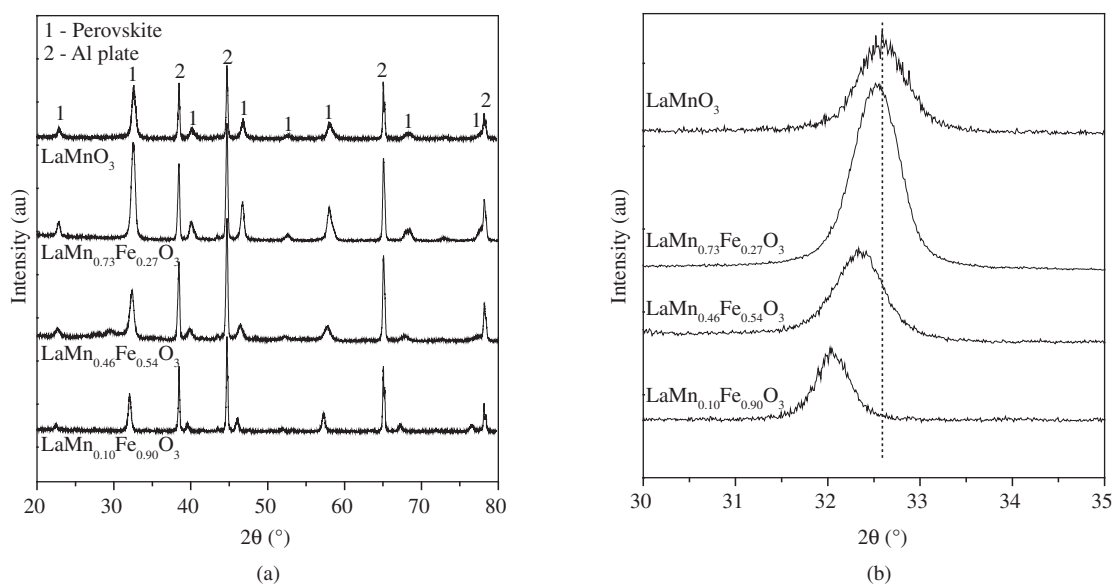

Figure 1. a) XRD of the perovskites $LaMn_{1-x}Fe_xO_3$, and b) shift of the XRD peak at ca. 32.5° s.
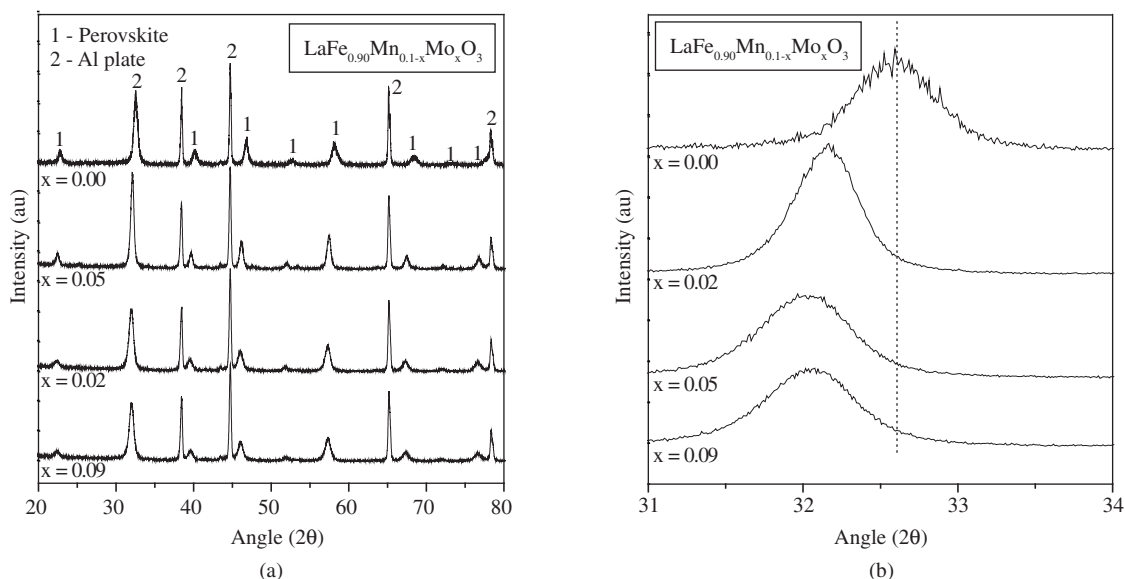

Figure 2. a) XRD of the different $LaMn_yFe_xMo_zO_3$ perovskites, and b) shift of the XRD peaks.

difractons angles as the Mo content increaased (Figure 2b) suggesting the incorporation of Mo into the structure. Both crystallite size and BET surface area did not change significantly for the series LaMn$_{1-x}$Fe$_x$O$_3$ and LaMn$_{0.1-x}$Fe$_{0.90}$Mo$_x$O$_3$ varying between 120-144 nm and 11-15 m^2 g^{-1}.

Mössbauer spectra of the LaMn$_{1-x}$Fe$_x$O$_3$ and LaMn$_{0.1-x}$Fe$_{0.90}$Mo$_x$O$_3$ perovskites are shown in Figure 3, with the hyperfine parameters in Table 1.

The spectra of LaMn$_{0.73}$Fe$_{0.27}$O$_3$ and LaMn$_{0.46}$Fe$_{0.54}$O$_3$ perovskites showed only doublets with isomer shift (δ) 0.33 mm/s, quadrupolar splitting (Δ) 0.52 mm/s and δ 0.33 mm/s, Δ 0.62 mm/s, likely related to octahedric Fe^{3+} dispersed in the perovskite structure. As seen in Figure 3a, the spectrum splits into sextets for higher concentration

Table 1. Mössbauer hyperfine parameters for the LaMn$_{1-x}$Fe$_x$O$_3$ and LaMn$_{0.1-x}$Fe$_{0.90}$Mo$_x$O$_3$ perovskites.

Perovskite	δ (mm/s) ± 0.05	Δ, ε (mm/s) ± 0.05	H$_{Hf}$(T) ± 0.05	Area (%) $\pm 1\%$
LaMn$_{0.73}$Fe$_{0.27}$O$_3$	0.33	0.52	-	100
LaMn$_{0.46}$Fe$_{0.54}$O$_3$	0.33	0.62	-	100
LaMn$_{0.10}$Fe$_{0.90}$O$_3$	0.37	–0.05	51.3	47
	0.37	0.05	49.2	53
LaMn$_{0.08}$Fe$_{0.90}$Mo$_{0.02}$O$_3$	0.36	–0.05	50.9	36
	0.37	0.09	48.4	64
LaMn$_{0.05}$Fe$_{0.90}$Mo$_{0.05}$O$_3$	0.36	–0.05	50.0	43
	0.37	0.04	46.1	50
	0.23	0.62	-	7
LaMn$_{0.01}$Fe$_{0.90}$Mo$_{0.09}$O$_3$	0.36	–0.05	49.8	53
	0.37	0.05	45.4	40
	0.23	0.61	-	7

ε quadrupole shift, δ isomer shift, Δ quadrupole splitting and H$_{hf}$ Hyperfine field.

of Fe. The LaMn$_{0.10}$Fe$_{0.90}$O$_3$ perovskite, for example, shows a signal with hyperfine parameters at δ 0.37 mm/s, ε -0.05 mm/s and magnetic hyperfine field (H$_{hf}$) 51.3 T with a relative area of 47%, assigned to the well crystallized LaFeO$_3$ structure. A second sextet at δ 0.37 mm/s, ε 0.05 mm/s and H$_{hf}$ 49.2 T is also observed with a relative area of 53%. This is identified as the poorly crystallized LaFeO$_3$[17,18] probably due to small particle size or to the presence of Mn.

The results for the Mo containing LaMn$_{0.08}$Fe$_{0.90}$Mo$_{0.02}$O$_3$ perovskite are very similar (Figure 3b), but the relative intensity of the more crystalline phase is lowered to 36% (δ 0.36 mm/s, ε –0.05 mm/s and H$_{hf}$ 50.9 T) with a slight increase to 64% of the poorly crystallized phase (δ 0.37 mm/s, ε 0.09 mm/s and H$_{hf}$ 48.4 T). These results suggest that the introduction of Mo into the perovskite structure induces a loss of crystallinity. The presence of higher Mo concentration apparently induces a more significant disorder in the perovskite structure producing a segregation of Fe^{3+} species detected as an additional signal at δ 0.23 mm/s, Δ 0.62 mm/s with a small relative spectral area of 7%.

Temperature Programmed Reduction (TPR) experiments were performed to investigate the reducibility of the different perovskites. TPR profile for LaMnO$_3$ (Figure 4) showed two sets of peaks: Peak 1 at 300-530 °C assigned to the reduction of Mn^{4+} and some Mn^{3+} and Peak 2 at temperatures higher than 600 °C due to the reduction of Mn^{3+} to produce MnO according to the Equation 2:[10]

$$2LaMnO_{3-x} + nH_2 \rightarrow La_2O_3 + 2MnO + nH_2O \qquad (2)$$

This TPR profile is similar to the previously published results for LaMnO$_3$.[8] TPR of the LaMn$_{0.46}$Fe$_{0.54}$O$_3$ sample (Figure 4) exhibit the same Peak 1 reduction features, but two important characteristics have changed: Peak 2 shifted to lower temperature (~700 °C) with a significant decrease in the peak area and a new reduction feature appeared starting at temperatures near 800 °C. The latter is likely related to the reduction of the Fe species. Thus, the reduction of iron and the
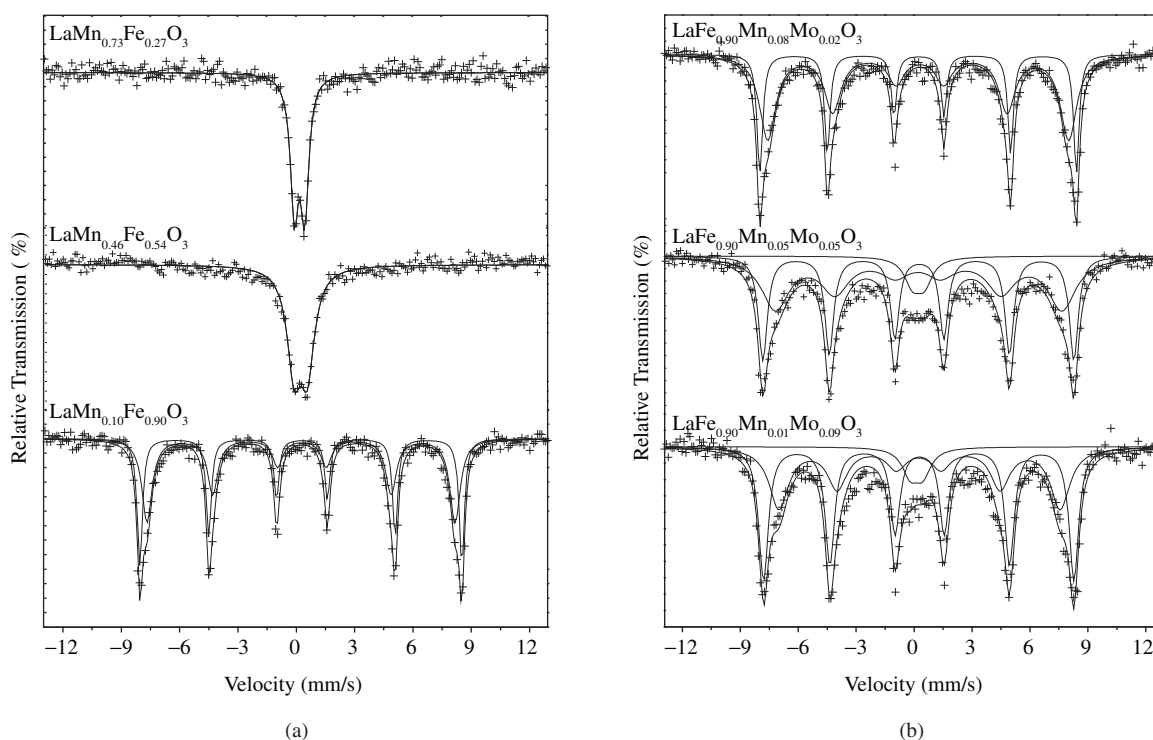

Figure 3. Room-temperature Mössbauer spectra of a) LaMn$_{1-x}$Fe$_x$O$_3$ and b) LaMn$_{0.1-x}$Fe$_{0.90}$Mo$_x$O$_3$ perovskites.

formation of Fe^o seem to occur only at temperature above 800 °C, which is when the perovskite structure collapses. Such remarkable thermal stability of iron in the perovskite structure has already been documented in the literature[18-19]. The smaller peaks for TPR spectra of D, E and F samples (Figure 4) in the temperature range 300-600 °C are likely related to the reduction of the molybdenum and manganese species present only in small amount.

3.2. Hydrogen peroxide decomposition and oxidation of the dye methylene blue

The catalytic activity of the perovskites $LaMn_{1-x}Fe_xO_3$ and $LaMn_{0.1-x}Fe_{0.90}Mo_xO_3$ was studied using two reactions: the H_2O_2 decomposition to O_2 ($H_2O_2 \rightarrow H_2O + 0.5O_2$); and the oxidation of the dye methylene blue a model contaminant with H_2O_2 in aqueous medium.
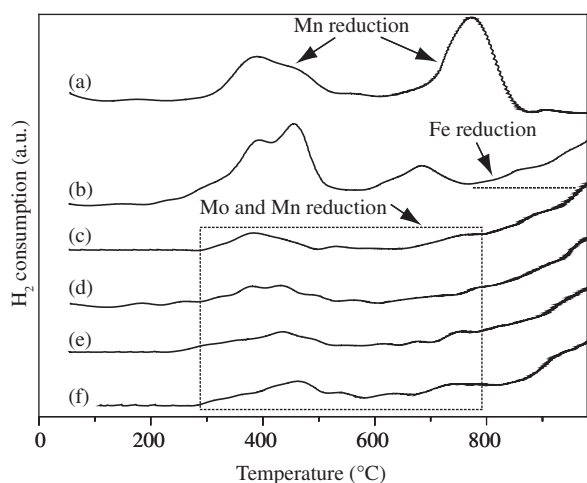
Figure 4. Temperature programmed reduction (TPR) spectra of a) $LaMnO_3$, b) $LaMn_{0.46}Fe_{0.54}O_3$, c) $LaMn_{0.10}Fe_{0.90}O_3$, d) $LaMn_{0.08}Fe_{0.90}Mo_{0.02}O_3$, e) $LaMn_{0.05}Fe_{0.90}Mo_{0.05}O_3$, and f) $LaMn_{0.01}Fe_{0.90}Mo_{0.09}O_3$.
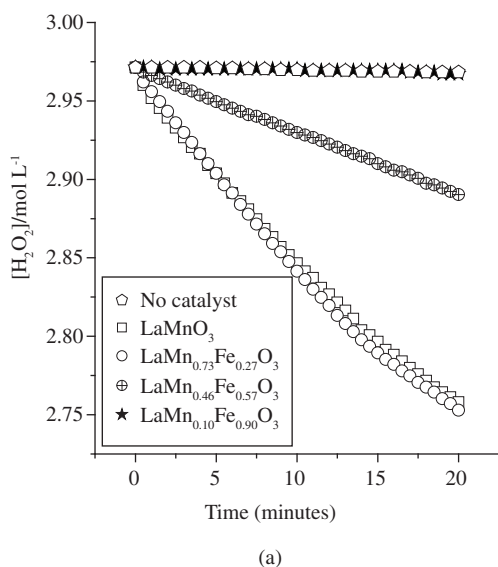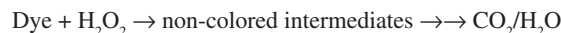
Figure 5 shows the H_2O_2 decomposition in the presence of different perovskites $LaMn_{1-x}Fe_xO_3$ and $LaMn_{0.1-x}Fe_{0.90}Mo_xO_3$. It is interesting to observe that the reactions without catalyst and the reactions in the presence of $LaMn_{0.10}Fe_{0.90}O_3$ and $LaMn_{0.1-x}Fe_{0.90}Mo_xO_3$ perovskites did not show catalytic activity for the H_2O_2 decomposition. On the other hand, when the Fe concentration in the perovskite decreased, i.e. $LaMn_{0.46}Fe_{0.54}O_3$ $LaMn_{0.73}Fe_{0.27}O_3$, and finally $LaMnO_3$, the activity increased significantly. The linear behavior of the H_2O_2 decomposition plots suggests a pseudo zeroth order kinetics under the reaction conditions studied. The reaction rates were calculated by the slope of the decomposition curves (Figure 6).

From Figure 6a it is possible to observe that the presence of small amounts of iron in the perovskite structure ($Fe_{0.27}$) led to an increase on the H_2O_2 decomposition rate (k_{dec}). On the other hand, it is observed a significant decrease of the H_2O_2 decomposition rate for the perovskite with higher Fe concentration ($Fe_{0.57}$ e $Fe_{0.90}$). Figure 6b shows that the rates of the H_2O_2 decomposition in the presence of $LaMn_{0.1-x}Fe_{0.90}Mo_xO_3$ were very low and did not vary significantly.

Although the mechanism of this reaction is not clear, the results suggested that the presence of manganese in the perovskite structure plays an important role in the catalytic activity, once their substitution by Fe and/or Mo induced a significant decrease on the H_2O_2 decomposition rate.

For the oxidation studies it was used the dye methylene blue as probe molecule. Methylene blue shows several interesting features as a probe molecule for oxidation reactions, such as: i) high solubility in water, ii) the oxidation can be monitored simply by spectrophotometric measurements, and iii) it simulates the behavior of textile dyes which are an important class of contaminant.

The reaction was monitored by the discoloration which is related to the first oxidation steps to produce non-colored intermediates:

$$Dye + H_2O_2 \rightarrow non\text{-}colored\ intermediates \rightarrow\rightarrow CO_2/H_2O$$

The discoloration activities in the presence of the perovskites $LaMnO_3$ and $LaMn_{0.1-x}Fe_{0.90}Mo_xO_3$ are shown in Figure 7. Preliminary tests of adsorption showed that these perovskites does not adsorb significantly the dye methylene blue and the adsorption process did not interfere the discoloration results.
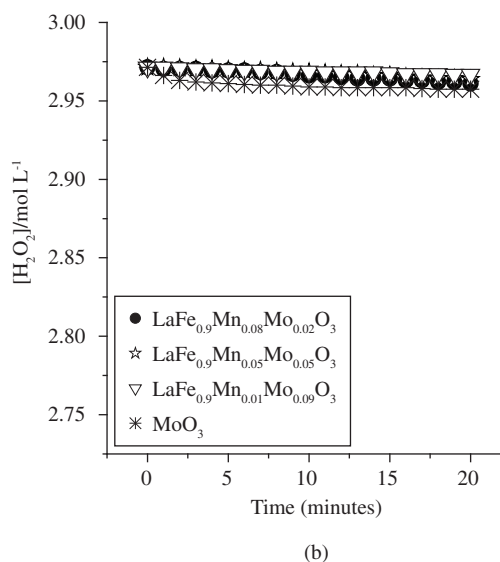
(a)

(b)

Figure 5. Hydrogen Peroxide decomposition in the presence of different perovskites $LaMn_{1-x}Fe_xO_3$, and $LaMn_{0.1-x}Fe_{0.90}Mo_xO_3$ ([H_2O_2] = 2.7 mol L^{-1}, pH = 5.5 ± 0.2, catalyst 30 mg).
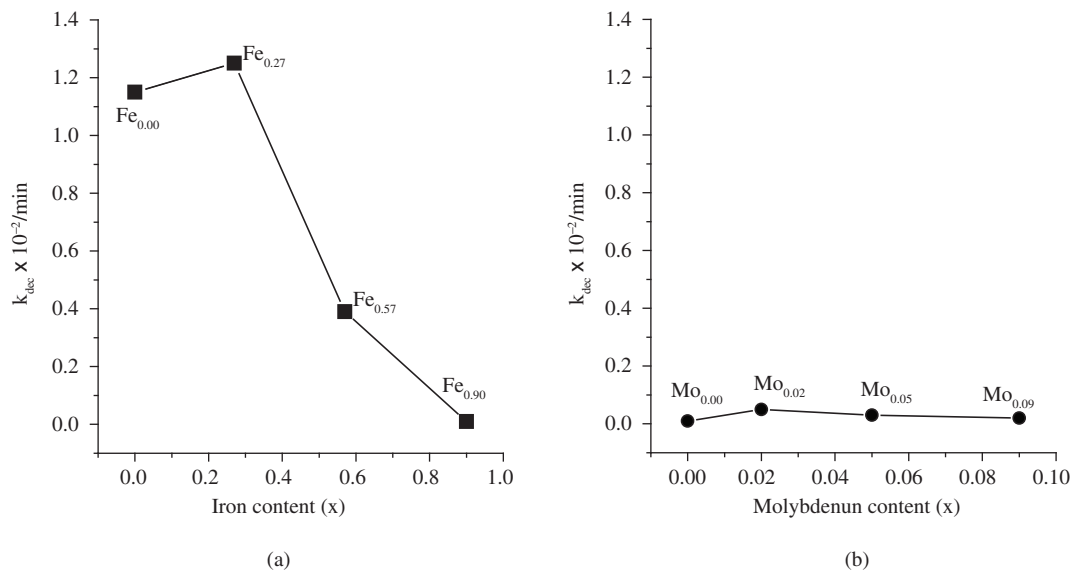
(a)　　　　　　　　　　　　　　　　　(b)

Figure 6. Hydrogen peroxide decomposition rate a) in the presence of perovskite with different concentration of Fe (LaMn$_{1-x}$Fe$_x$O$_3$), and b) different concentration of Mo (LaMn$_{0.1-x}$Fe$_{0.90}$Mo$_x$O$_3$).
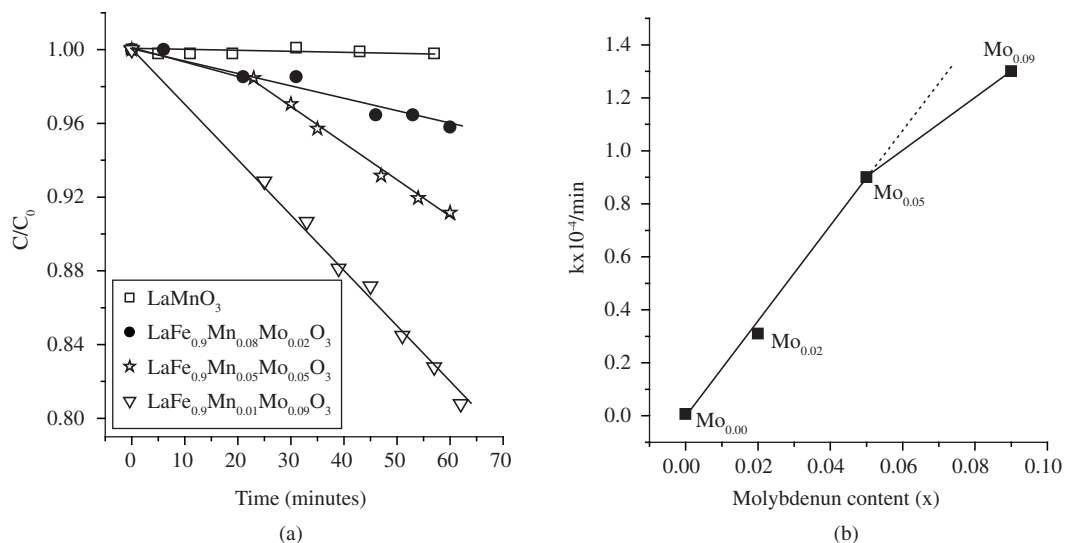

(a)　　　　　　　　　　　　　　　　　(b)

Figure 7. a) Discoloration of the dye methylene blue (0.1 g L^{-1}) with H$_2$O$_2$ in the presence of LaMn$_{0.1-x}$Fe$_{0.90}$Mo$_x$O$_3$ (28 °C, 30 mg, [H$_2$O$_2$] = 2.9 mol L^{-1}), and b) Methylene blue discoloration rate as function of the Mo content in the LaMn$_{0.1-x}$Fe$_{0.90}$Mo$_x$O$_3$.

It is interesting to observe that the perovskite LaMnO$_3$ did not present catalytic activity for the methylene blue discoloration. However, the presence of Mo in the perovskite (LaMn$_{0.1-x}$Fe$_{0.90}$Mo$_x$O$_3$) led to an increase on the activity. The linear behavior of the methylene blue discoloration plots again suggested a pseudo zeroth order kinetics. The methylene blue discoloration rates (k$_{discol}$) are shown in the Figure 7b.

From Figure 7b it is clear that the k$_{discol}$ increases with the Mo content in the perovskite structure. It is interesting to observe from Figure 7b, that this increase is linear up to Mo content of 0.05 (Mo$_{0.05}$). Although, the role of Mo to improve dye oxidation is not clear, one can envisage that surface Mo can activate H$_2$O$_2$ to form surface peroxomolybdenium complexes active for oxidation processes. These surface complexes can react directly with the dye molecule or can react with H$_2$O to form highly reactive HO* radicals[24].

4. Conclusion

The results obtained by XRD and Mössbauer spectroscopy showed that Fe and Mo can be incorporated in the perovskite structure. The addition of Fe to the series LaMn$_{1-x}$Fe$_x$O$_3$ caused a decrease on the H$_2$O$_2$ decomposition activity. The perovskites LaMn$_{0.1-x}$Fe$_{0.90}$Mo$_x$O$_3$ did not show any significant catalytic activity for the H$_2$O$_2$ decomposition. On the other hand, for the heterogeneous Fenton reactions, the reaction rate increased with the Mo concentration.

Acknowledgements

References

1. Tao S, Irvine JTS, Kilner JA. An Efficient Solid Oxide Fuel Cell Based upon Single-Phase Perovskites. *Advanced Materials.* 2005; 17(14):1734-1737.

2. Kim J, Hwang DW, Kim HG, Bae SW, Lee JS, Li W, Oh SH. Highly Efficient Overall Water Splitting Through Optimization of Preparation and Operation Conditions of Layered Perovskite Photocatalysts. *Topics in Catalysis.* 2005; 35(3-4): 295-303.

3. Ichimura K, Inoue Y, Yasumori I. Hydrogenation and hydrogenolysis of hydrocarbons on perovskite oxides. *Catalysis Reviews - Science and Engineering.* 1992; 34(4):301-20.

4. Isupova LA, Sutormina EF, Kulikovskaya NA, Plyasova LM, Rudina NA, Ovsyannikova IA, Zolotarskii IA, Sadykov VA. Honeycomb supported perovskite catalysts for ammonia oxidation processes. *Catalysis Today.* 2005; 105(3-4):429-435.

5. Liu ZM, Hao JM, Fu LX, Zhu TL. Study of $Ag/La_{0.6}Ce_{0.4}CoO_3$ catalysts for direct decomposition and reduction of nitrogen oxides with propene in the presence of oxygen. *Applied Catalysis B: Environmental.* 2003; 44(4):355-370.

6. Keane, MA. Ceramics for catalysis. *Journal Of Materials Science.* 2003; 38(23):4661-4675.

7. Pena MA, Fierro JLG. Chemical Structures and Performance of Perovskite Oxides. *Chemical Reviews.* 2001; 101(7):1981-2018.

8. Yi N, Cao Y, Su Y, Dai WL, He HY, Fan KN. Nanocrystalline $LaCoO_3$ perovskite particles confined in SBA-15 silica as a new efficient catalyst for hydrocarbon oxidation. *Journal of Catalysis.* 2005; 230(1):249-253.

9. Stephan K, Hackenberger M, Kiessling D, Wendt G. Total Oxidation of Methane and Chlorinated Hydrocarbons on Zirconia Supported $A_{1-x}Sr_xMnO_3$ Catalysts. *Chemical Engineering & Technology.* 2004; 27(6):687-693.

10. Lee YN, Lago RM, Fierro JLG, Cortes V, Sapina F, Martinez E. Surface properties and catalytic performance for ethane combustion on $La_{1-x}K_xMnO_{3+}\delta$ perovskites. *Applied Catalysis, A: General.* 2001; 207(1,2):17-24.

11. Lago RM, Moura FCC, Araujo MH, Ardisson JD, Macedo WA, Albuquerque AS. Investigation of the solid state reaction of $LaMnO_3$ with $Fe°$ and its effect on the catalytic reactions with H_2O_2. *Journal of the Brazilian Chemical Society.* 2007; 18(2):322-329.

12. Popa M, Frantti J, Kakihana M. Lanthanum ferrite $LaFeO_{3-}\delta$ nanopowders obtained by the polymerizable complex method. *Solid State Ionics.* 2002; 154-155;437-445.

13. Lee YN, Lago RM, Fierro JLG, Gonzalez J. Hydrogen peroxide decomposition over $Ln_{1-x}A_xMnO_3$ (Ln = La or Nd and A = K or Sr) perovskites. *Applied Catalysis, A: General.* 2001; 215(1-2):245-256.

14. Lee YN, Lago RM, Fierro JLG. Surface properties and catalytic performance for ethane combustion on $La_{1-x}K_xMnO_{3+}\delta$ perovskites. *Applied Catalysis, A: General.* 2001; 207(1,2):17-24.

15. Wandekar RV, Wani BN, Bharadwaj SR. High temperature phase transition in $Sm_{0.95}MnO_{2.925}$. *Journal of Alloys and Compounds.* 2007; 437(1-2):53-57.

16. Naray-Szabo S, The structural type of perovskite ($CaTiO_3$). *Naturwissenschaften.* 1943; 31:202-3.

17. Islam MS, Cherry M, Catlow CRA. Oxygen diffusion in $LaMnO_3$ and $LaCoO_3$ perovskite-type oxides: a molecular dynamics study. *Journal of Solid State Chemistry.* 1996; 124(2):230-237.

18. Berry FJ, Ren X, Marco JF. Reduction properties of perovskite-related rare earth orthoferrites. *Czechoslovak Journal of Physics.* 2005; 55(7):771-780.

19. Zhong Z, Chen K, Ji Y, Yan Q. Methane combustion over B-site partially substituted perovskite-type $LaFeO_3$ prepared by sol-gel method. *Applied Catalysis, A: General.* 1997; 156(1):29-41.

20. Sinquin G, Petit C, Hindermann JP, Kiennemann A. Study of the formation of $LaMO_3$ (M = Co, Mn) perovskites by propionates precursors: application to the catalytic destruction of chlorinated VOCs. *Catalysis Today.* 2001; 70(1-3):183-196.

21. Poplawski K, Lichtenberger J, Keil FJ, Schnitzlein K, Amiridis MD. Catalytic oxidation of 1,2-dichlorobenzene over ABO_3-type perovskites. *Catalysis Today.* 2000; 62(4):329-336.

22. Sinquin G, Petit C, Libs S, Hindermann JP, Kiennemann A. Catalytic destruction of chlorinated C2 compounds on a $LaMnO_{3+}$ perovskite catalyst. *Applied Catalysis, B: Environmental.* 2001; 32(1-2):37-47

23. Spinicci R, Tofanari A, Delmastro A, Mazza D, Ronchetti S. Atalytic properties of stoichiometric and non-stoichiometric $LaFeO_3$ perovskite for total oxidation of methane. *Materials Chemistry and Physics.* 2002; 76(1):20-25.

24. Gutiérrez JLG, Fuentes GA, Terán MEH, García P, Guevara FM, Cruz FJ. Ultra-deep oxidative desulfurization of diesel fuel by the Mo/Al_2O_3-H_2O^2 system: The effect of system parameters on catalytic activity. *Applied Catalysis, A: General.* 2008; 334(1-2):366-373.